FRACTURE MECHANICS COMPUTATIONS WITH MSC/PROBE

Michael J. Heskitt
The MacNeal-Schwendler Corporation
St. Louis Office
1600 S. Brentwood Blvd., Suite 840
St. Louis, Mo. 63144
Tel: (314)961-6960 Fax: (314)962-4295

ABSTRACT

Methods based on linear elastic fracture mechanics are of great importance in evaluating the strength and durability of structural and mechanical systems. The Finite Element Method (FEM) has become increasingly popular for fracture mechanics computations, and many commercial FEM packages now contain fracture mechanics capabilities. The fracture mechanics capabilities of the p-version finite element program, MSC/PROBE, are discussed and several example applications are used for illustration. Particular emphasis is placed on the quality of the results, and the methods that are available to verify the solution accuracy.

TABLE OF CONTENTS

1.0 Introduction

Methods based on linear elastic fracture mechanics are of great importance in evaluating the strength and durability of structural and mechanical systems. The Finite Element Method (FEM) has become increasingly popular for fracture mechanics computations, and many commercial FEM packages now contain fracture mechanics capabilities. Assessing the quality and reliability of the FEM results has always been a difficult and tedious task. Global energy, local error indicators, and convergence of the appropriate functionals, must all be checked to determine the accuracy of the FEM solution. These procedures are often neglected in production environments due to time constraints, and thus the quality of the finite element solution is often dependent on the experience of the analyst.

MSC/PROBE contains fracture mechanics extraction procedures developed specifically for the p-version of the finite element method. These techniques are extremely efficient and easy to use. This, along with the explicit quality control features, provides an excellent tool for performing fracture mechanics analyses and verifying the accuracy of the results. This report discusses the quality control procedures in **MSC/PROBE** and demonstrates both planar and solid fracture mechanics computations through examples.

2.0 Quality Control in MSC/PROBE

To be complete, quality control procedures in the FEM must contain some form of an evaluation of the error in the overall strain energy, the local contribution of errors by elements, and the convergence of the data of interest. Proper evaluation of these conditions is very laborious and hence impractical with conventional h-version FEM programs. **MSC/PROBE** includes features which make these tests easy and straightforward to perform. Each of the quality control procedures are discussed in the following sections, and selected tests are demonstrated in the example problems.

2.1 Estimated Error in the Energy Norm

MSC/PROBE automatically provides a sequence of solutions, corresponding to increasing polynomial degree (p-level) shape functions, from which an estimate of the exact strain energy can be obtained. This estimated exact strain energy is then compared to the strain energy of the current p-level solution and the error in the energy norm is computed. The estimated relative error in the energy norm provides feedback to the overall convergence of the model. It does not, however, reflect the solution quality on a local level. Therefore, this is a necessary but not sufficient check that must be augmented by the local quality control procedures described next.

2.2 Elemental Equilibrium and Stress Continuity Between Elements

Tabulated data displaying elemental freebody information is provided by **MSC/PROBE**. The freebody data is not the nodal force balance h-version programs customarily provide (which will trivially balance), but rather the integral of the stress vector components computed from the finite element solution along the element boundaries. The relative imbalance in equilibrium for each

element, and the continuity of the force resultants along common edges or faces of elements are indicators of the quality of the mesh. If these values are approximately the same for each element, (with respect to each interelement boundary), then the mesh is well designed. This type of feedback is not generally provided from h-version programs.

2.3 Convergence of Functionals of Interest

To increase the accuracy of the solution in the FEM, whether using h-version, p-version or a combination of the two, the number of Degrees of Freedom (DOF) of the model must be increased in what is called an extension process. Without performing an extension process, no estimate can be made as to how close the data of interest, (i.e. δ, σ, ε, K_I, K_{II}, etc.), computed from the finite element solution is to the same data computed from the exact solution. Local error indicators may help guide decisions on where to refine a mesh or where to increase the p-level, but they cannot provide quantitative information on the accuracy of the data computed from the finite element solution. Because **MSC/PROBE** automatically provides a sequence of solutions, where the number of DOF increase with the p-level of each element, convergence through the p-extension process can be examined. As such, the convergence of any functional can be shown. This provides the most powerful method for evaluating the solution accuracy available.

3.0 Planar Fracture Mechanics

MSC/PROBE-PLANAR consists of modules that allow the analysis of plane stress, plane strain, or axisymmetric problems. In each case, a crack configuration can be modeled and automatic extraction procedures can be used to obtain the stress intensity factors, the strength of the singularity, and the energy release rates. Special superconvergent extraction techniques are used. No special "crack tip" elements are needed in the vicinity of the crack tip. Rather, meshing guidelines, including grading in geometric progression towards the crack tip, are used. A discussion of the extraction techniques follows, and the meshing guidelines are discussed in connection with the example problems.

3.1 Extraction Techniques for Planar Models

Two new algorithms, called **The Contour Integral Method (CIM)** and **The Cutoff Function Method (CFM)**, have been implemented in **MSC/PROBE**. The familiar **Energy Release Rate Method (ERRM)** is also provided.

The **CIM** and the **CFM** are extremely efficient extraction techniques that will separate the Mode I and Mode II stress intensity factors. The methods employ contour and area integrals to extract K_I and K_{II}. A complete description of these methods is beyond the scope of this report but can be found in [1]. The present implementation restricts their use to models with constant thickness (inside the integral path only), with isotropic materials, and where no thermal loading or body forces are present.

The **ERRM**, as implemented in **MSC/PROBE**, uses the Parks Stiffness Derivative Method [2]. The crack length is increased by a small amount and the change in the local elemental stiffnesses are used to estimate the change in the strain

energy, ΔU. This is then divided by the change in crack area, ΔA, for the Energy Release Rate ($\mathcal{G}$):

$$\mathcal{G} = \Delta U/\Delta A \qquad (1)$$

The magnitude of the stress intensity vector is then calculated from $\mathcal{G}$ using the relation [3],

$$|\vec{K}| = \sqrt{K_I^2 + K_{II}^2} = \sqrt{\frac{\mathcal{G}\, E}{(1-\nu^2)}} \quad (\text{psi}\sqrt{\text{in}}) \quad \text{for Plane Strain,} \qquad (2.a)$$

or

$$|\vec{K}| = \sqrt{K_I^2 + K_{II}^2} = \sqrt{\mathcal{G}\, E} \quad (\text{psi}\sqrt{\text{in}}) \quad \text{for Plane Stress,} \qquad (2.b)$$

where E is the Modulus of Elasticity and ν is Poisson's ratio for the material.

Computationally, the **ERRM** is somewhat less efficient than either the **CIM** and the **CFM**, and it does not separate K_I and K_{II}, but it can be used for almost any crack/model configuration without restrictions on the thickness, materials, or loading conditions. All three methods will converge to the same results, although the **CFM** has been shown to converge more rapidly than the other two methods [1].

3.2 Planar Example Problem: Cracked Panel Subjected to Shear and Tension

3.2.1 Problem Description

The first fracture mechanics example discussed in this paper is a large flat panel with a crack located near one edge. The panel is loaded in tension (normal to the crack) as well as in shear. The panel configuration, material properties, and loading are shown in Figure 3.1.

This problem contains both Mode I and Mode II excitations of the crack. The crack half-length, (a), will be varied from .2 inches to .8 inches to illustrate the convenient procedures provided within **MSC/PROBE** for investigating the stress intensity variation with crack length.

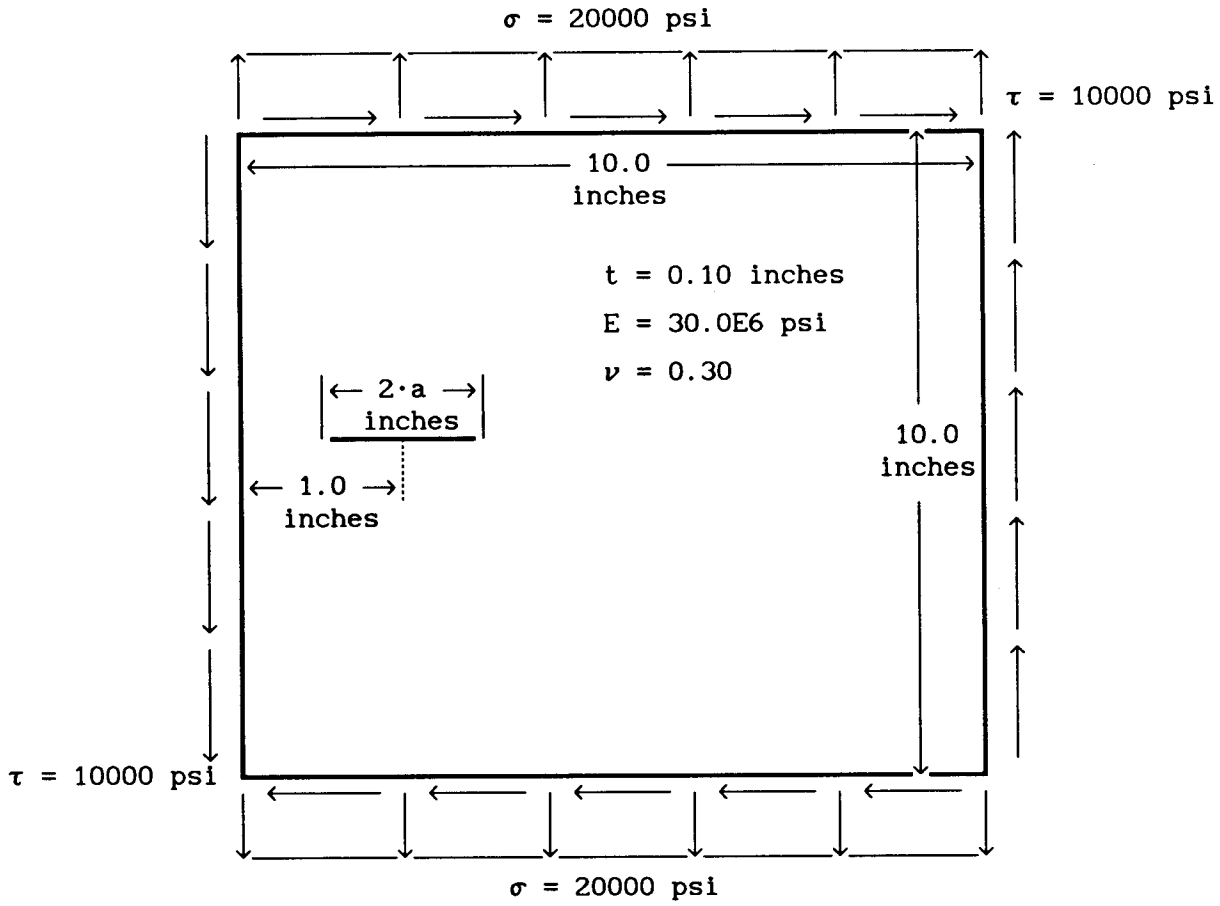

FIGURE 3.1: CRACKED PLATED SUBJECTED TO SHEAR AND TENSION

3.2.2 Mesh Design and Boundary Conditions

Meshing fracture mechanics problems with traditional h-version programs is inherently cumbersome due to the stringent restrictions that are placed on the size and shape of an h-version element. This makes transitions from important areas with high stress gradients (i.e. in the locale of a crack tip or stress concentration) to the surrounding regions difficult, with many elements (and DOF) "wasted" in the transition zones. At the crack tip, special quarter point, or singular, elements are often employed to improve the approximation.

By employing the p extension process on properly designed meshes, the rate of convergence is much faster than in the case of the h-version. An important added benefit is that the elements may have much higher aspect ratios. In fracture mechanics applications, this allows far simpler meshes with fewer elements to be used. Also, no special elements are necessary at the crack tip.

The mesh for this example is shown in Figure 3.2. The complete mesh required only 42 elements. Figure 3.3 shows the areas surrounding the two crack tips magnified. Geometric grading ratios were used to focus the DOF at the crack tips. Grading ratios of 7:1 to 10:1 were used in the two rings of elements

surrounding the tip. Two rings, used in this manner, will be sufficient in most cases to assure exponential convergence of the strain energy, and quality results from the fracture mechanics extraction techniques. Many cases will require only one ring of elements.

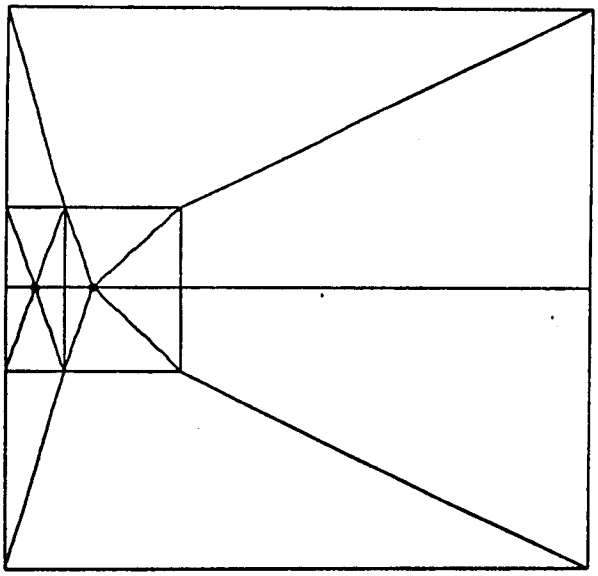

FIGURE 3.2: MSC/PROBE MESH FOR THE CRACKED PLATE

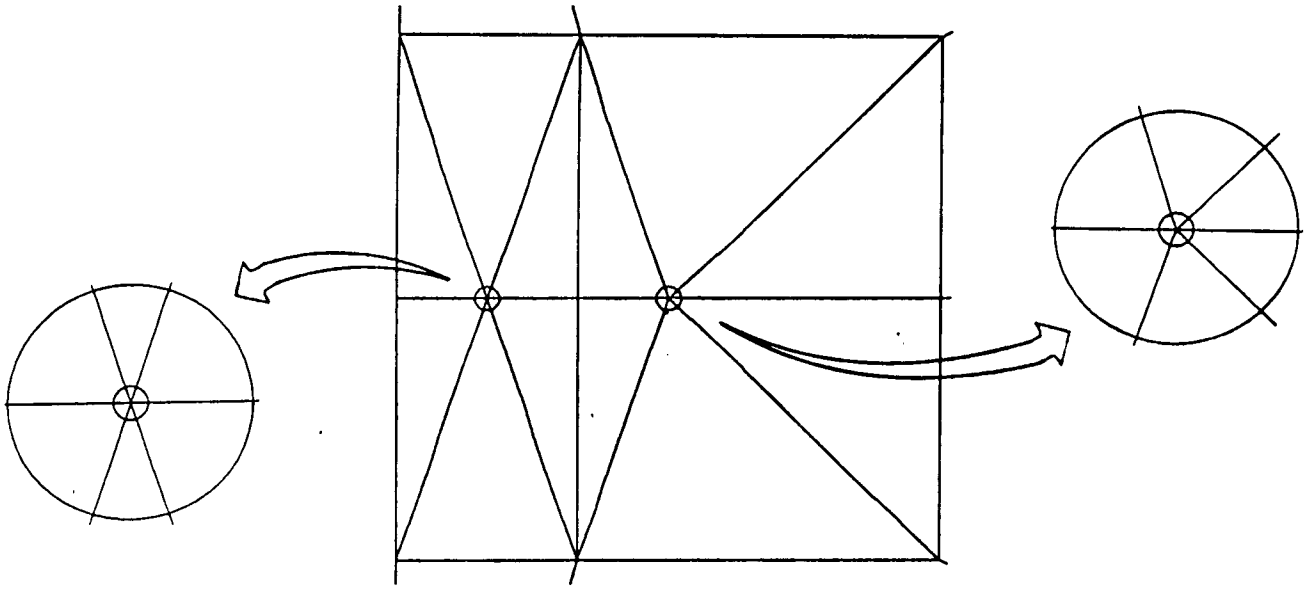

FIGURE 3.3: DETAILS OF THE CRACK TIP REGION

The tension and shear loading were applied as tractions along the outer element boundaries. In this case, only constant tractions were required, but **MSC/PROBE** allows traction inputs of CONSTANT, FORMULA, or INTERPOLATION, so a great deal of flexibility is provided for load inputs. The loading for this problem is self equilibrating, so constraints are needed only to restrict rigid body motion. These were applied at two of the corner nodes.

3.2.3 Model Checkout and Solution Verification

The tests performed to establish that the discretization errors were reasonably small are described in this section.

The first check is for the convergence of the strain energy. Figure 3.4 shows a plot of the strain energy and the estimated percent error in the energy norm provided in **MSC/PROBE**. The estimated percent error in the energy norm at a p-level of 8 is 0.29%. This indicates that the overall accuracy of the finite element solution is well within the range normally expected in engineering computations. This strong convergence in the strain energy is typical for p-extensions on geometrically graded meshes.

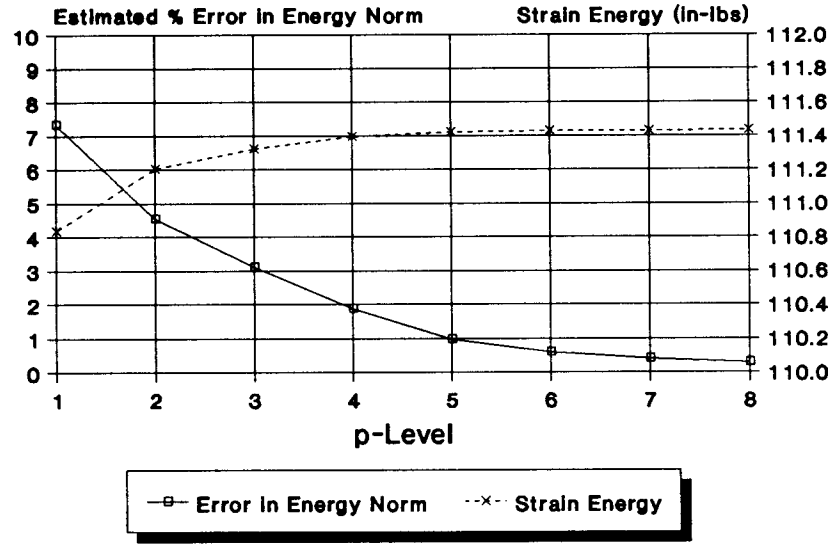

FIGURE 3.4: ENERGY CONVERGENCE FOR THE CRACKED PANEL

The next global check is simply to view the deformed shape to assure that the loads were applied in the proper directions and positions. Figure 3.5 shows the deformed shape of the model. The deformed shape is as would be expected for this type of loading.

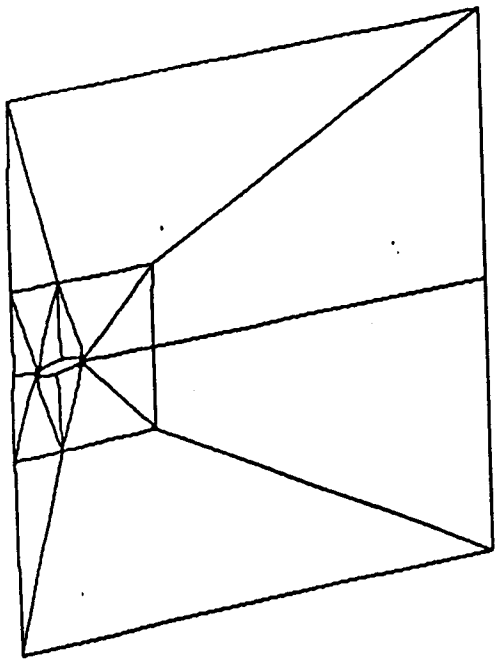

FIGURE 3.5: DEFLECTED SHAPE FOR THE CRACKED PANEL

Several local quality checks were performed before accepting the results. The first was to investigate the continuity of the stresses along the element boundaries. This was done using the *Elemental Stress Report* provided in **MSC/PROBE**. Another method of visualizing this effect is by using stress contour plots. **MSC/PROBE** does not average the stress results along elemental boundaries. The results, shown in Figure 3.6, show that, at element boundaries, several small discontinuities occur. A "perfect" solution would display no discontinuities in the contour plots. The contour plot shown in Figure 3.6 is close to this ideal case. Note that the contour was limited to exclude the gradients in the local vicinity of the crack tips for a better display of the contours remote from this region. The contour plot also serves to verify that no reactions are generated at the rigid body constraints. If the applied loads were not in equilibrium, and reactions were generated at the points where the rigid body constraints were applied, we would see local stress concentrations at the constrained points because the nodal constraints would be singular points.

Another local check of the solution quality is the elemental equilibrium. This was investigated via the *Element Freebody Report* provided by **MSC/PROBE**. All the elements not directly connected to the singular points were found to have less than 1% error in the equilibrium.

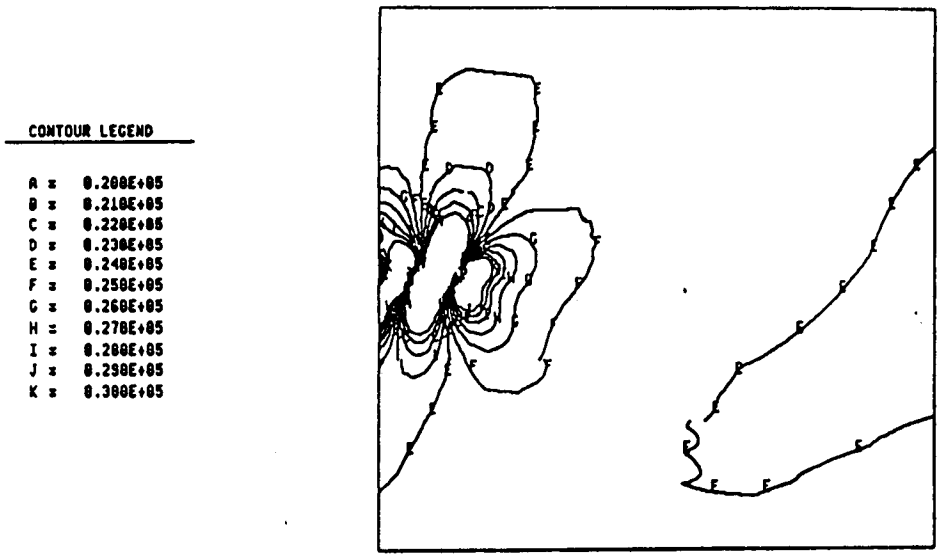

FIGURE 3.6: MAXIMUM PRINCIPAL STRESS CONTOUR PLOT FOR THE CRACKED PANEL

The last and most definitive check of the local solution quality, is to investigate the convergence of the functional of interest. Here we are interested in the Mode I and Mode II stress intensity factors at the end of the crack nearest to the panel edge. All three extraction methods available in **MSC/PROBE** were used to compare the results for the 1.0 inch crack length. These are shown in Table 3.1 and a graph of $|\vec{K}|$ for the three methods is included in Figure 3.7. The solutions from all three methods at a p-level of 8 agree to within 0.1%. These results are much more accurate than the results from [3] where K_I = 27300 (psi $\sqrt{in}$) and K_{II} = 13700 (psi $\sqrt{in}$).

	CIM			CFM			ERRM
PLEVEL	K_I	K_{II}	$\vec{K}$	K_I	K_{II}	$\vec{K}$	$\vec{K}$
1	36334	12455	38409	29082	9787	30684	32172
2	27012	12322	28690	29761	13782	32797	32748
3	29228	14383	32575	28036	13890	31288	31368
4	27867	13627	31020	28290	13889	31515	31433
5	28414	13820	31596	28217	13724	31377	31311
6	28056	13655	31202	28140	13704	31299	31253
7	28197	13736	31364	28157	13715	31319	31286
8	28127	13704	31287	28145	13713	31307	31281

(Units in psi $\sqrt{in}$)

TABLE 3.1: CONVERGENCE OF STRESS INTENSITY FACTORS FOR THE CRACKED PANEL WITH A 1.0" CRACK

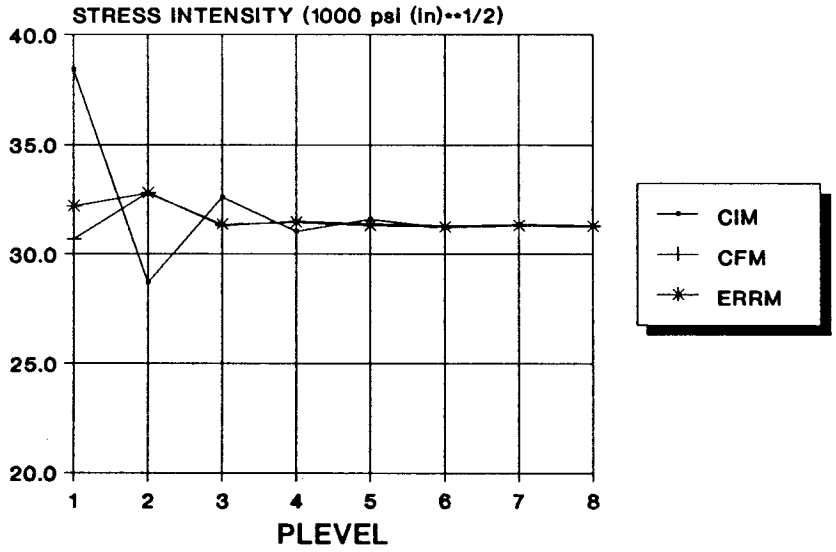

FIGURE 3.7: CONVERGENCE OF THE STRESS INTENSITY VECTOR FOR THE CRACKED PANEL

3.2.4 Stress Intensity Variation with Crack Length

A study of the change in the stress intensity factors as the crack grows is greatly facilitated by some of the features in **MSC/PROBE**. If the circles enclosing the two rings of elements at each crack tip (See Figure 3.3) are defined relative to local coordinate systems at each crack tip, then the cracks can be "grown" by simply changing the location of the two local coordinate systems. The nodes and elements around the crack tip are associated with these circles, so they will move along with the new tip locations. No new mesh is required because the p-version elements are tolerant of large aspect ratios and skew.

The crack length was varied from 0.2 inches to 0.8 inches, and was centered at 1.0 inch from the panel edge. Details of the resulting mesh for the two extreme cases are shown in Figure 3.8. The results for the Mode I and Mode II stress intensity factors vs. the crack length are shown in Figure 3.9. Also shown are the results from [3] for comparison.

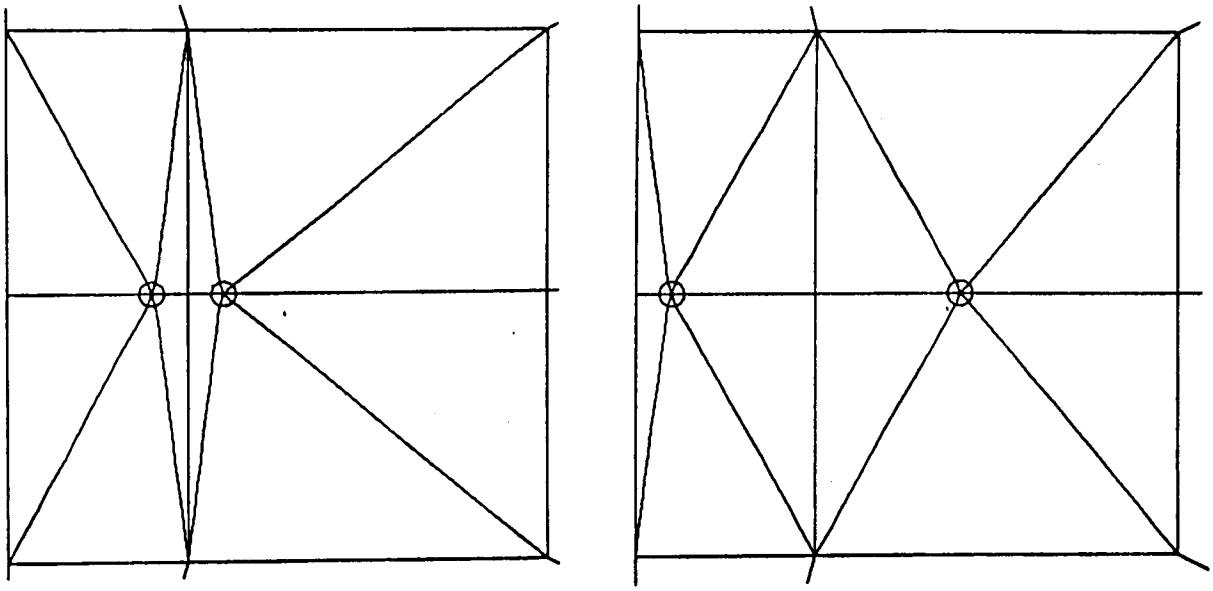

CRACK LENGTH = 0.2 INCHES CRACK LENGTH = 0.8 INCHES

FIGURE 3.8: CRACK TIP MESH DETAILS FOR THE SMALLEST AND LARGEST CRACK SIZES IN THE CRACK LENGTH VARIATION STUDY

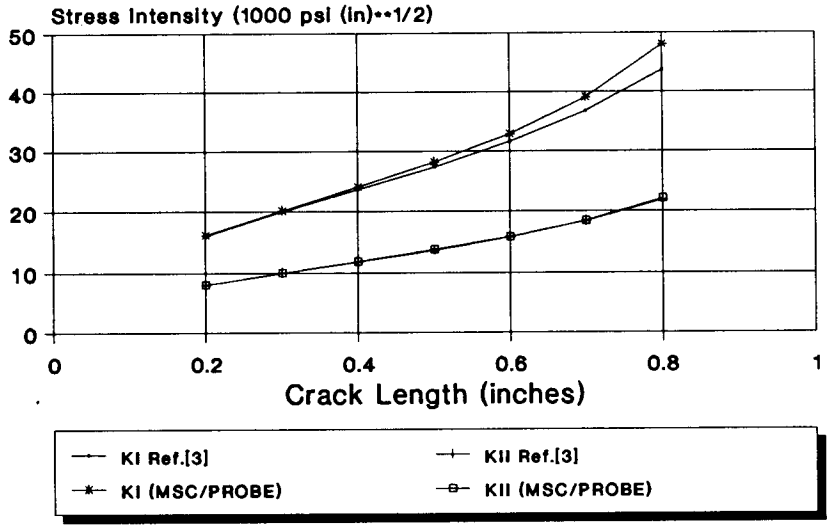

FIGURE 3.9: STRESS INTENSITY RESULTS VS. CRACK LENGTH

3.3 Axisymmetric Example Problem: Rod with a Circular Penny Crack

3.3.1 Problem Description

The next fracture mechanics example is a circular bar with an imbedded penny shaped crack. The crack is normal to the centerline of the bar. The bar is

loaded in uniaxial tension so only Mode I excitation will occur. A cross section of the bar is shown in Figure 3.10. The applied traction at the upper and lower surface is 20000 psi. The material is steel.

This is actually a solid fracture mechanics problem, but the **AXISYMMETRIC** module in **MSC/PROBE-PLANAR** was used. This allows problems of this nature to be solved quickly, with far simpler meshes and less man-time and computer resources than would be needed with a fully solid model. General solid fracture mechanics problems are addressed in Chapter 4.

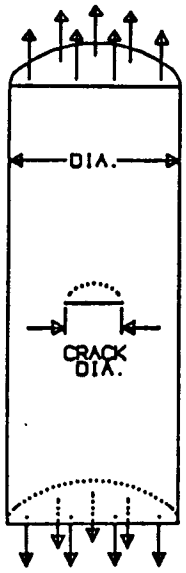

FIGURE 3.10: CIRCULAR BAR WITH PENNY SHAPED CRACK

3.3.2 Mesh Design and Boundary Conditions

The **AXISYMMETRIC** module in **MSC/PROBE-PLANAR** was used for this problem. The model is constructed as the cross section or generating surface that would be swept through 360^{o} to generate the complete solid volume. **MSC/PROBE** then uses a one radian slice of the solid model for the analysis. Therefore, for example, if a 1 psi traction (p) were applied to the upper surface of a cylinder with an outside radius, r_o, the total force that acts on the cylinder is

$$F_{Total} = p\pi r_o^2 \ (\text{lbf}) \qquad (3)$$

and the resulting force that will be reported for that "edge" of the model (actually the 1 radian face) is

$$F_{Radian} = \frac{F_{Total}}{2\pi} = \frac{pr_o^2}{2} \ (\text{lbf/radian}) \qquad (4)$$

Meshing guidelines similar to the previous example were used, but in this case, symmetry conditions were employed to reduce the model size. A typical mesh is shown in Figure 3.11 along with a magnification of the crack tip detail. For this problem symmetric boundary conditions are used along the lower face outside the crack front. The left edge is the axis centerline for the bar.

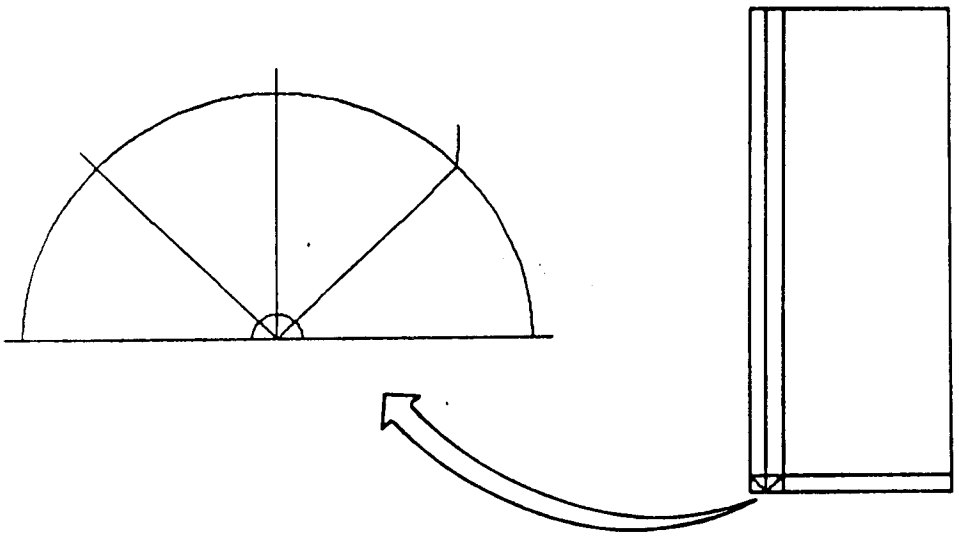

FIGURE 3.11: MSC/PROBE MESH FOR THE CRACKED BAR

3.3.3 Model Checkout and Solution Verification

Essentially the same procedures as in the first example were used for model checkout and solution verification. The results for the case with a rod diameter of 10 inches and an imbedded crack diameter of 0.2 inch (a/r = 0.02) will be shown here. Other cases with increasing crack-size/rod-diameter ratios are presented in the next section.

The strain energy convergence and estimated error in the energy norm are shown in Figure 3.12. Again, excellent convergence was obtained with the percent relative error estimated at 0.05% for the p-level of 8. We should note that it is not necessary to obtain the entire sequence of solutions, to p=8, allowed by **MSC/PROBE**. Good engineering accuracy is obtained in this case by p=5 or p=6. The entire sequence is shown here for purposes of illustration.

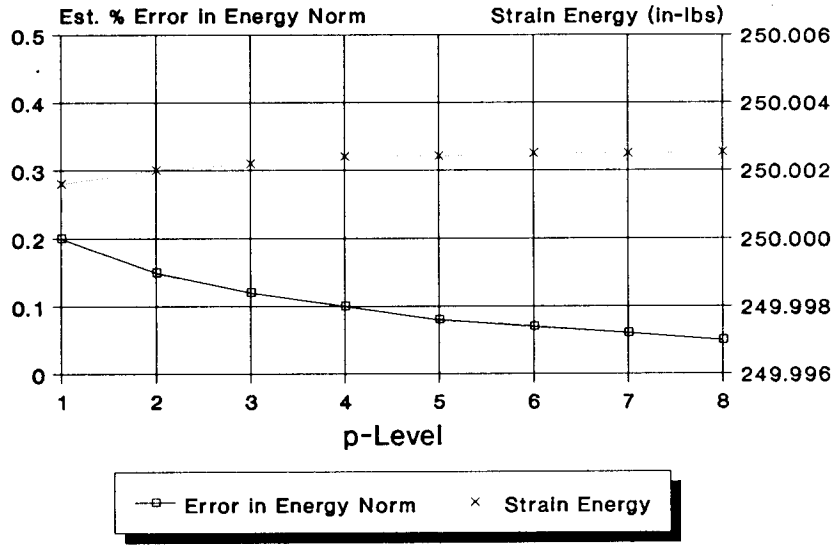

FIGURE 3.12: ENERGY CONVERGENCE FOR THE CRACKED ROD

The deflected shape of the local area around the crack tip is shown in Figure 3.13. The Mode I displacements are apparent in this figure.

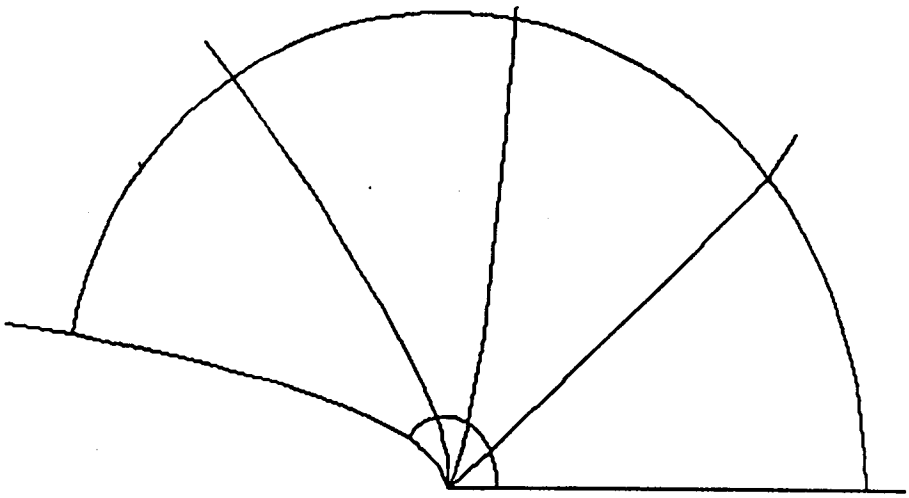

FIGURE 3.13: DEFLECTED SHAPE OF THE CRACK FACE

Again, other local indicators were checked to assure the validity of the local solution. These included elemental equilibrium from the *Element Freebody Report* and continuity of stresses between elements using the *Element Stress Report* and contour plots. Lastly, the convergence of the stress intensity vector magnitude, $|\vec{K}|$, was checked and is shown in Figure 3.14. In this case, since K_{II}= 0.0, K_I= $|\vec{K}|$, and the **ERRM** was used to extract the results (The **CIM** and **CFM** are not available in the **AXISYMMETRIC** Module). The **ERRM** uses the plane strain assumption for calculating $|\vec{K}|$ from the energy release rate in the **AXISYMMETRIC** Module.

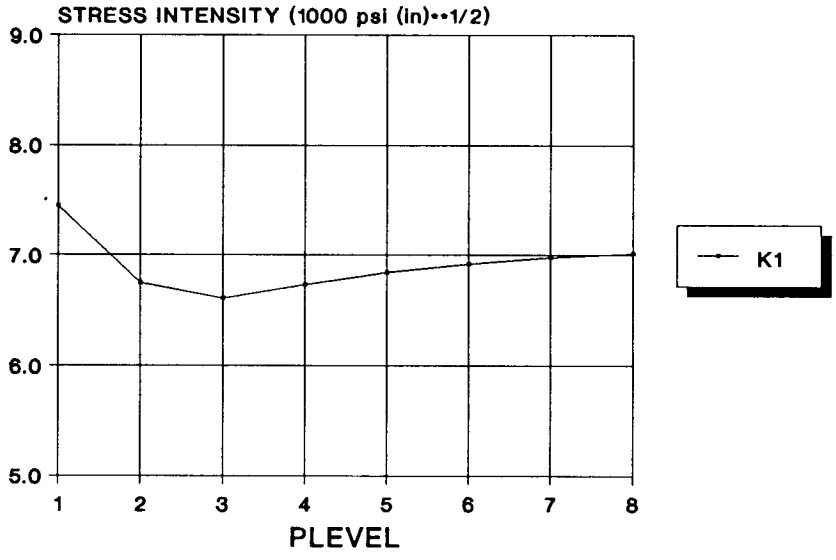

FIGURE 3.14: K_I CONVERGENCE FOR A 10" DIA ROD WITH A 0.1" DIA CENTER CRACK

3.3.4 Stress Intensity Variation with Crack Length

To study the effect of the crack diameter to rod diameter ratio (a/r) on the stress intensity factor, several **MSC/PROBE** models were run. In the previous example, the crack was grown by simply moving a local coordinate system located at the crack tip. In this case, the outer diameter of the rod, which was defined as a line, is moved towards the centerline, while keeping the crack tip constant, to increase the ratio of the crack size to the rod diameter. The resulting mesh for the two extreme cases and one intermediate case are shown in Figure 3.15. The results from the crack length variation are shown in Figure 3.16 and are compared with results from [3]. Once again, the results obtained from **MSC/PROBE** are more accurate than those presented in [3].

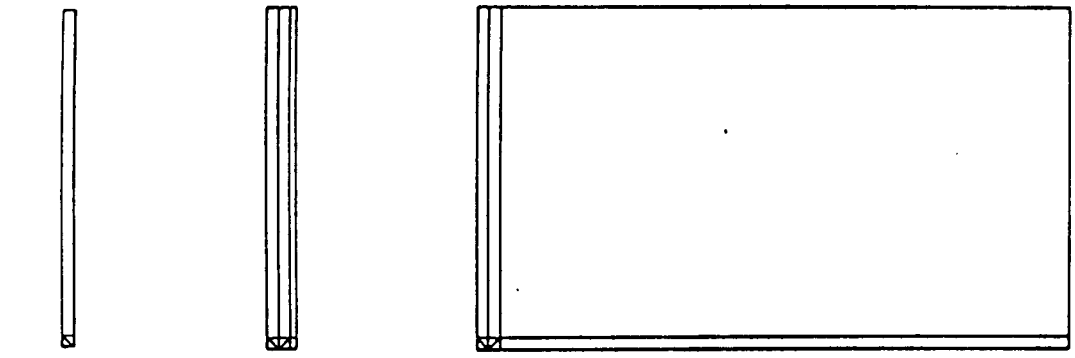

FIGURE 3.15: MSC/PROBE MESHES FOR CRACK LENGTH VARIATION OF ROD MODELS

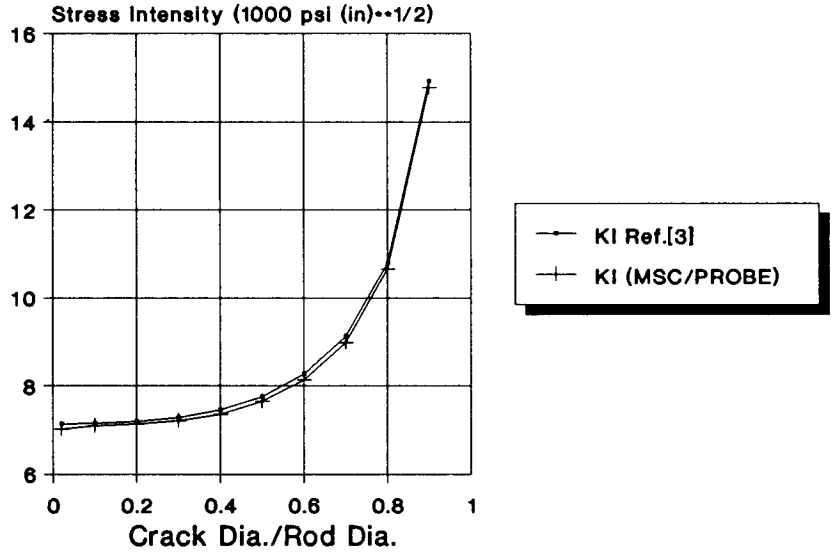

FIGURE 3.16: STRESS INTENSITY RESULTS VS. CRACK LENGTH FOR THE ROD

4.0 Solid Fracture Mechanics

MSC/PROBE can also be used for fracture mechanics analysis of solids. One case, the axisymmetric problem, although analyzed using the AXISYMMETRIC module in **MSC/PROBE-PLANAR**, represents a solid fracture mechanics problem. More general solid problems can be analyzed using **MSC/PROBE-SOLID**. Although in the current release there are no automatic extraction capabilities for stress intensity factors for solid problems, several methods may be used to extract fracture mechanics results reliably with a reasonable amount of effort. One method is discussed in the next section, and demonstrated with an example.

4.1 Extraction Techniques for Solid Models

Several aspects of the p-version, and features in **MSC/PROBE** make possible the construction of simple meshes for solid crack problems. The robust nature of the p-version allows larger aspect ratios and skew angles which greatly facilitate transitioning from the area around a crack tip to the surrounding regions. This is especially important in three dimensions. Also, the smooth nature of the solution and the ability to examine the convergence of the displacement and stress data at any point within the model allows reliable use of the extraction methods. In general, complete quality control tests are extremely difficult to perform with traditional h-version programs and are rarely used in professional practice.

Equations of the stress and displacement distributions in the region around a crack were developed by Irwin (1957) based on the method of Westergaard (1939) and are repeated in [3] and [4]. Specifically, the displacement field along the crack face can be used to calculate the Mode I, Mode II, and Mode III stress intensity factors using the equations [3],

$$v = \frac{K_I}{G}\sqrt{\frac{r}{2\pi}}\,\sin\frac{\theta}{2}\left[\,2-2\nu-\cos^2\frac{\theta}{2}\,\right] + \text{Higher Order Terms} \qquad (5a)$$

$$u = \frac{K_{II}}{G}\sqrt{\frac{r}{2\pi}}\,\sin\frac{\theta}{2}\left[\,2-2\nu+\cos^2\frac{\theta}{2}\,\right] + \text{Higher Order Terms} \qquad (5b)$$

$$w = \frac{K_{III}}{G}\sqrt{\frac{r}{2\pi}}\,\sin\frac{\theta}{2} + \text{Higher Order Terms} \qquad (5c)$$

where G is the material Shear Modulus, θ is the angle measured from the extension of the crack face into the material (i.e. the x-axis), r is the distance from the crack tip, and the u, v, and w displacements follow the conventions of the x, y, and z axes, respectively, as shown in Figure 4.1. Equations (5a) and (5b) assume plane strain in the x-y plane and Equation (5c) assumes plane strain in the x-z plane. We note that the plane strain assumption is only an approximation to the fully three-dimensional case,

however, since fracture mechanics data are generated in essentially two-dimensional experiments, such approximations are generally accepted.

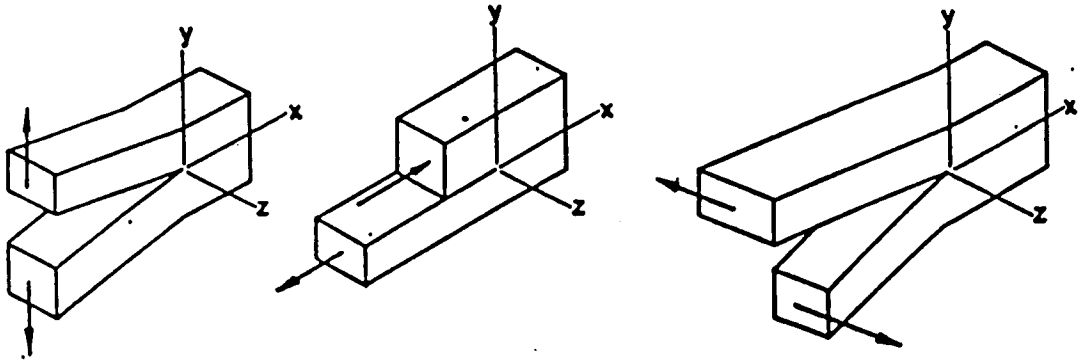

MODE I MODE II MODE III

FIGURE 4.1: BASIC MODES OF CRACK SURFACE DISPLACEMENTS

If the limit of equations (5) is taken as r→0, the higher order terms can be neglected. Equations (5) can then be rearranged to solve for K_i. Doing this and recognizing that on the crack face $\theta=180^{\circ}$, so $\cos(\theta/2)=0.0$ and $\sin(\theta/2)=1.0$, gives

$$K_I = \lim_{r\to 0} \left\{ \frac{vG}{(2-2\nu)} \sqrt{\frac{2\pi}{r}} \right\} \tag{6a}$$

$$K_{II} = \lim_{r\to 0} \left\{ \frac{uG}{(2-2\nu)} \sqrt{\frac{2\pi}{r}} \right\} \tag{6b}$$

$$K_{III} = \lim_{r\to 0} \left\{ wG\sqrt{\frac{2\pi}{r}} \right\} \tag{6c}$$

For plane stress (used where the crack front reaches a free surface) equations (5) and (6) are modified by replacing Poisson's ratio, ν, with $\nu/(1+\nu)$.

In the finite element method, one can only expect accurate results some finite distance away from the crack tip, which is a singularity. Therefore, to use this method, the analyst must be able to determine the zones where the finite element solution is inaccurate ("close" to the crack tip), and where the higher order terms become dominant ("far" from the crack tip). The region between these zones should be linear with respect to r, and can be used to extrapolate to r→0 for the stress intensities. This limiting process is displayed graphically in Figure 4.2.

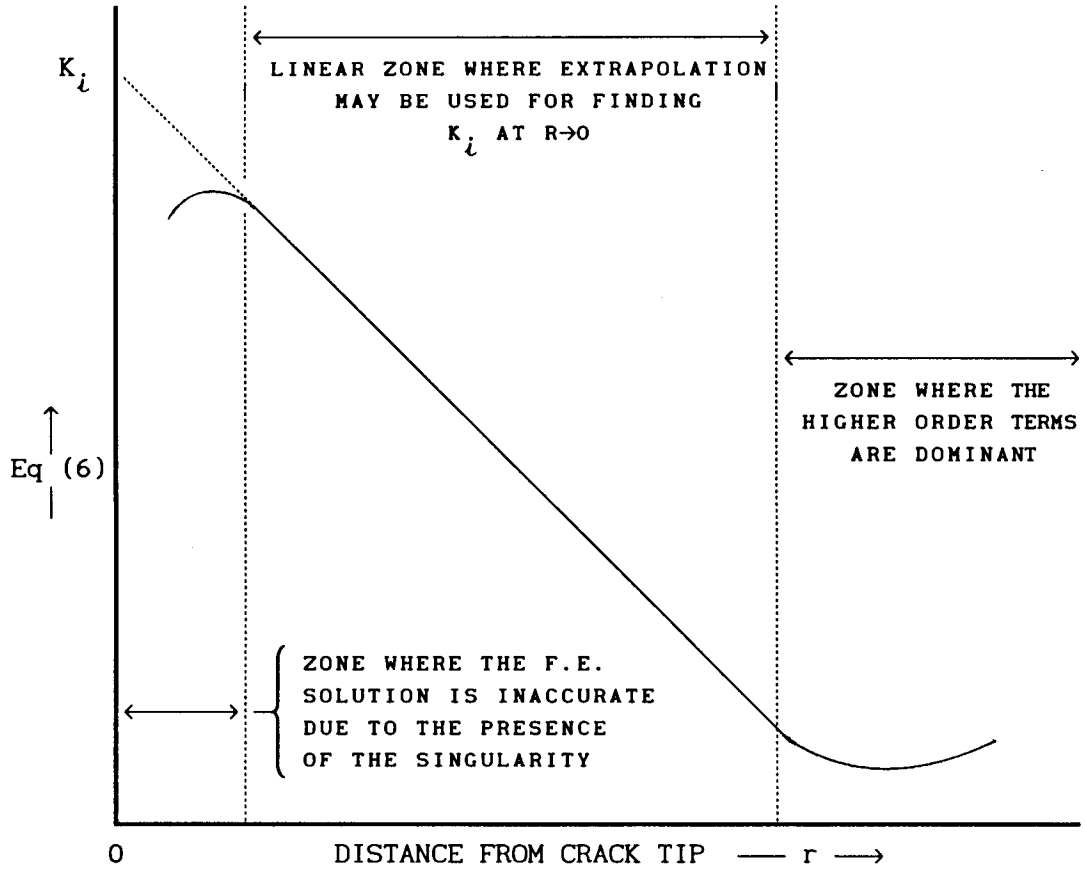

FIGURE 4.2: SCHEMATIC VIEW OF THE DISPLACEMENT METHOD FOR STRESS INTENSITY COMPUTATIONS

In **MSC/PROBE**, the displacements can be output along any line using any local coordinate system (in this case; in the crack plane starting at the point of interest on the crack tip and normal to the crack front). The results can then be multiplied by the appropriate factors in Eq. (6), and plotted as in Figure 4.2. The extrapolation can then be performed for the stress intensity factor. One very important feature is that the zone where the displacements are inaccurate can be readily identified by examining the convergence of the displacements as the p-level is increased. This procedure is demonstrated in the following example.

4.2 Solid Example Problem: Plate with an Elliptical Surface Crack

4.2.1 Problem Description

The solid fracture mechanics example problem consists of a large rectangular plate with a semi-elliptical surface crack. The plate is loaded in bi-axial tension and in-plane shear. The plate is 10.0 inches on each side and 0.40 inches thick. The crack is located on the centerline with a minor half-axis (into the plate thickness) of 0.10 inches and a major half-axis (on the plate surface) of 0.30 inches. See Figure 4.3 for the problem geometry. The applied tensile traction is 20000 psi and the applied shear traction is 10000 psi. The material is steel.

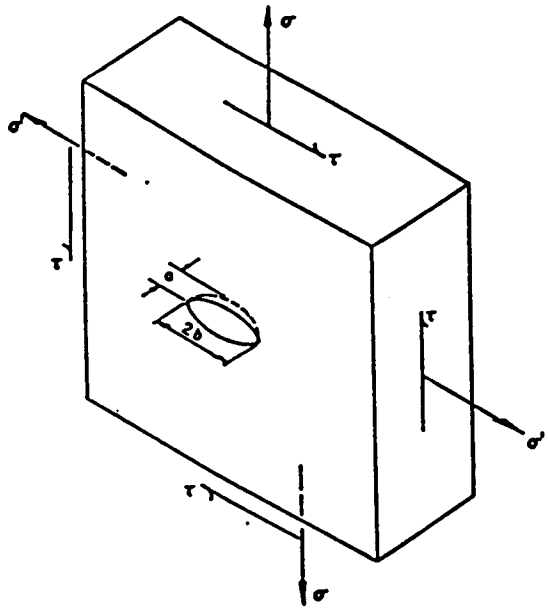

FIGURE 4.3: PLATE WITH A SEMI-ELLIPTICAL SURFACE CRACK

4.2.2 Mesh Design and Boundary Conditions

To allow only one quarter of the plate to be discretized, symmetric boundary conditions were used for the tension loading, and anti-symmetric conditions were used for the shear loading. The tension load parallel to the crack face does not excite any of the three modes, so it is ignored. The finite element mesh consists of 287 elements. The model is shown in Figure 4.4 with a magnification of the area around the crack tip. Figure 4.5 shows the bottom layer of elements along the crack face for more clarity.

Characteristic of p-version meshes, this model shows how rapid transitions can be made from a fine to a coarse mesh. This is especially important in solid models to reduce the number of DOF necessary for the analysis. Another method used to limit the number of DOF was to restrict the polynomial order of the elements in non-critical regions, while increasing the p-level in only the critical areas. **MSC/PROBE** allows predefined sets of elements to be assigned a fixed p-level. Here, elements removed from the crack zone were limited to a p-level of 2, while the p-level of the elements in the crack zone were increased from 1 to 6 to provide information on convergence. This kept the number of DOF for the model below 27,500 for the p-level of 6 solution. The higher p-levels of 7 and 8 were not necessary in this analysis, but if the error estimates and quality control procedures had indicated that greater accuracy was needed, then the higher p-levels could have been run without any changes to the mesh. Only if this last step proved inadequate would the analyst need to make mesh refinements.

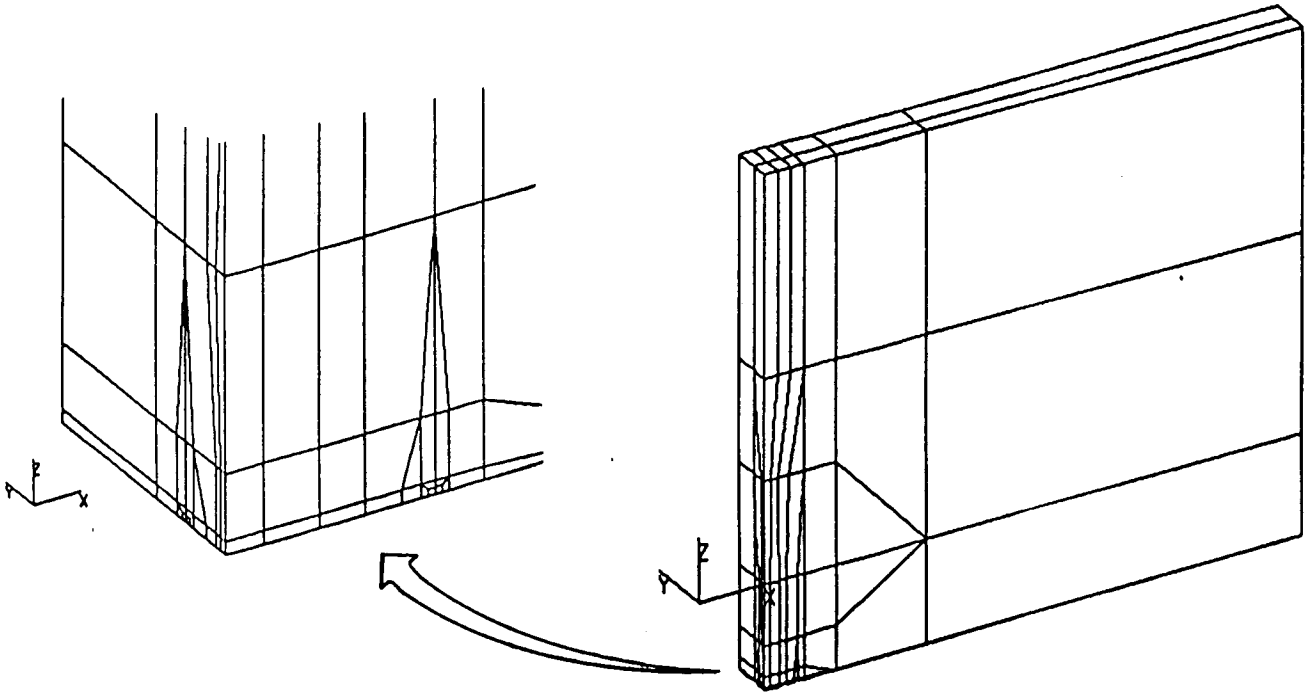

FIGURE 4.4: QUARTER MODEL OF THE PLATE WITH A SURFACE CRACK

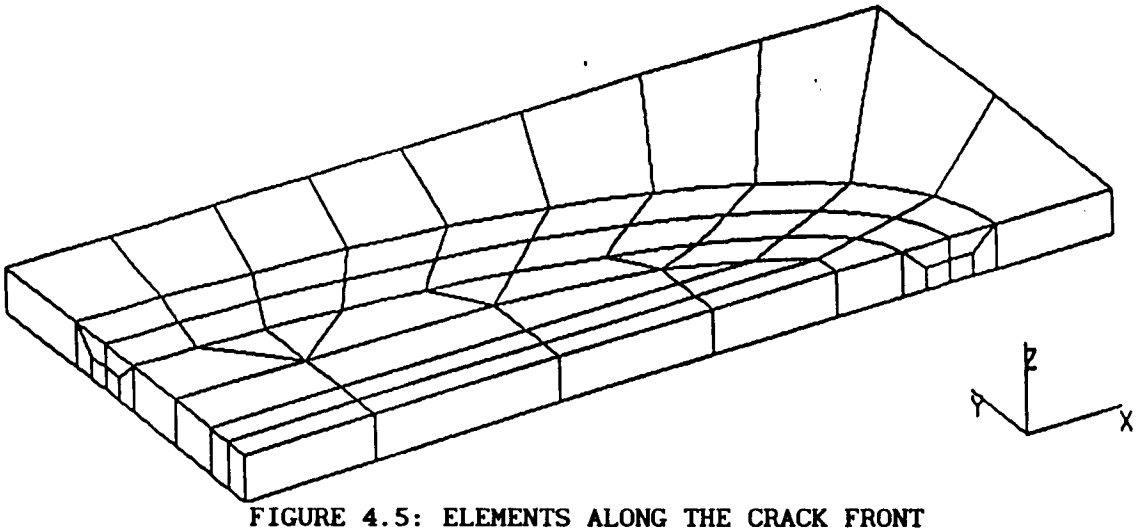

FIGURE 4.5: ELEMENTS ALONG THE CRACK FRONT

4.2.3 Model Checkout and Solution Verification

As in the planar examples, the first step in verifying the model is to look at the convergence of the strain energy. The estimated error in the energy norm is shown in Figure 4.6 for both the tension and shear load cases.

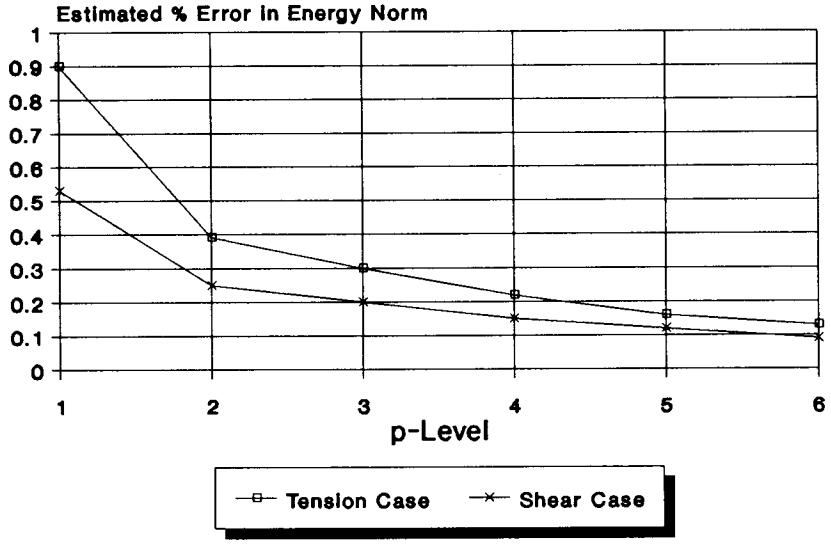

FIGURE 4.6: PERCENT ERROR IN THE ENERGY NORM FOR THE CRACKED PLATE

Another global check of the model is to view the displacements. The overall model displacements were as expected for each load case. Local displacements around the crack tip were also displayed to check proper constraints in the region. Figure 4.7 shows the bottom layer of elements around the crack tip under the tension loading. A refined "data recovery" grid is overlaid on the original p-version elements to allow better displacement visualization from the post-processing program. This is done automaticaaly from the plotting options in **MSC/PROBE**. The original p-version elements are shown in Figure 4.5.

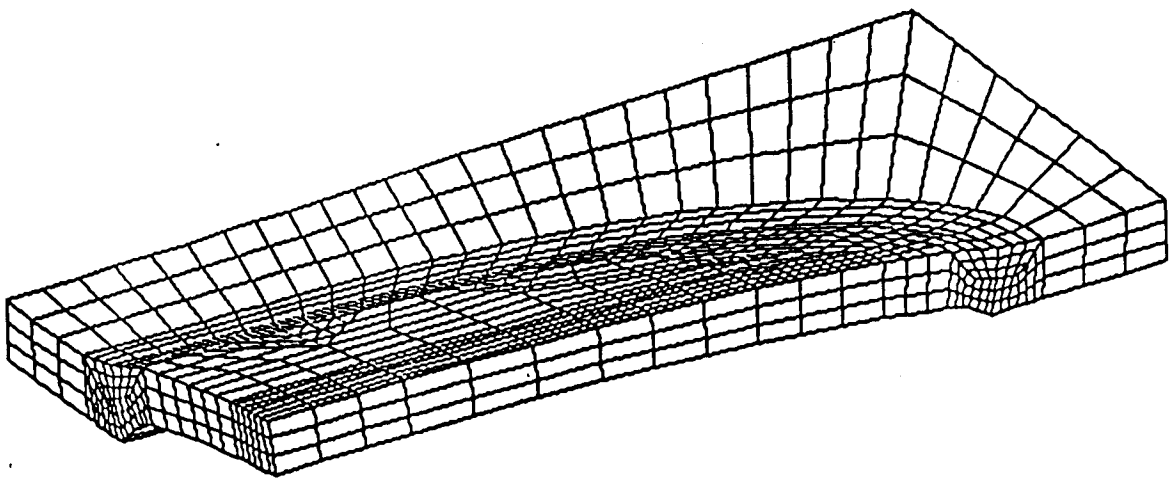

FIGURE 4.7: CRACK FACE DISPLACEMENTS UNDER TENSION LOAD

The elemental equilibrium and stress continuity between the elements were also investigated to assess the quality of the solution. The elements showing the highest percent force imbalance are near the crack front. This can be expected since the crack front is a strong singularity. The proper interpretation of this information is that if greater accuracy is needed in the data of interest, and this accuracy cannot be realized by p-extension, then these elements should be refined. For this particular analysis, the displacements in the region of the crack are the functionals of interest, since these will be used with Eq.(6) to determine the stress intensity factors. Therefore, establishing confidence in the displacement results near the crack tip is necessary.

To evaluate the displacements close to the crack tip, local coordinate systems were used and the displacements relative to the crack face were obtained in the local systems. The convergence of the displacements with respect to increasing p-level is shown in Figure 4.8 for the position along the centerline of the minor axis of the ellipse. Each line in Figure 4.8 represents the displacement convergence at a point of radius, R, from the crack tip, as the p-level is increased from 1 to 6. As can be seen, for the points closest to the tip (i.e. R=0.003 inches) the displacements have not converged. They continue to increase with the p-level. Further away from the crack (i.e. R>0.020 inches) the displacements have leveled off very well by a p-level of 6. This then establishes the quality of the converged displacements, and the regions within the domain where they have converged. This information is available for a single mesh and additional user interaction is not required.

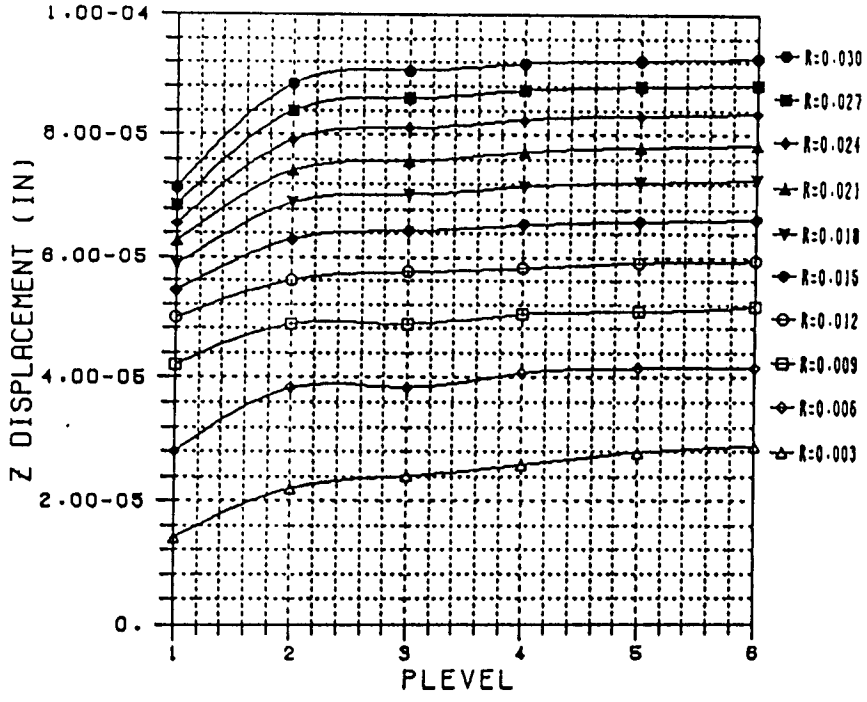

FIGURE 4.8: CONVERGENCE OF DISPLACEMENTS FOR POINTS ALONG THE CRACK CENTERLINE

4.2.4 RESULTS

Once the displacements have been verified, plots similar to Figure 4.2 can be generated at any position for which the stress intensity factors are desired. The plot of Eq.(6) versus the distance from the crack tip, R, is shown in Figure 4.9 for the crack centerline. Here the limiting process is displayed graphically as an extension of the linear portion of the curve to R=0.00 inches. The results for KI and KIII at the crack centerline are compared to References [4] and [5] in Table 4.1.

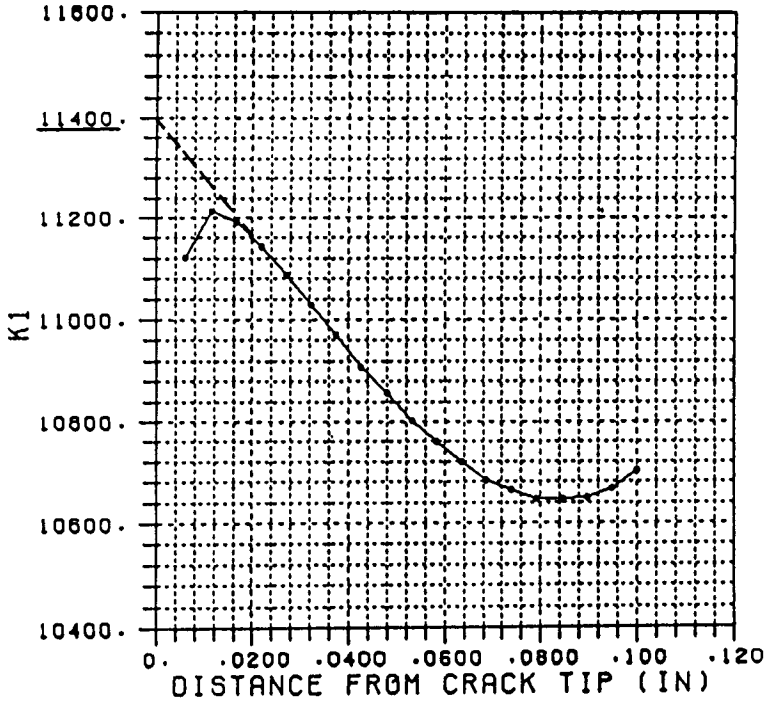

FIGURE 4.9: EQUATION 6 PLOT ALONG CRACK CENTERLINE

	MSC/PROBE	REF [4]	REF [5]
K_I	11400	11120	11840
K_{III}	5740	5150	N/A

TABLE 4.1: MODE I AND MODE III COMPARISONS AT CRACK CENTERLINE

This procedure was continued at various other points around the crack face for the Mode I Intensity Factors. It should be noted that the plane stress approximation that was used to develop Eq. (5), and (6) becomes less accurate as the free surface is approached. The behavior in this region becomes more three dimensional due to the gradients parallel to the crack front. As such, some of the plots of Eq. (6) from the region close to the free surface were not as well defined as those closer to the crack centerline (i.e. Figure 4.9). Reasonable extrapolations were obtained, though, and the results are shown in Figure 4.10 with Reference [5] as a comparison. The X axis coordinates are relative to the angle from the free face (ie. ϕ=0 at the free face, ϕ=π/2 at the centerline). The results from MSC/PROBE are generally less than 5% below

those from Reference [5] except at the free surface. Subsequent studies by some of the authors of [5], found in [6], showed behavior more similar to the results from MSC/PROBE in the region close to the free surface. Again, though, the behavior in this region is three dimensional in nature, and the limitations of the plane stress and plane strain assumptions should be recognized.

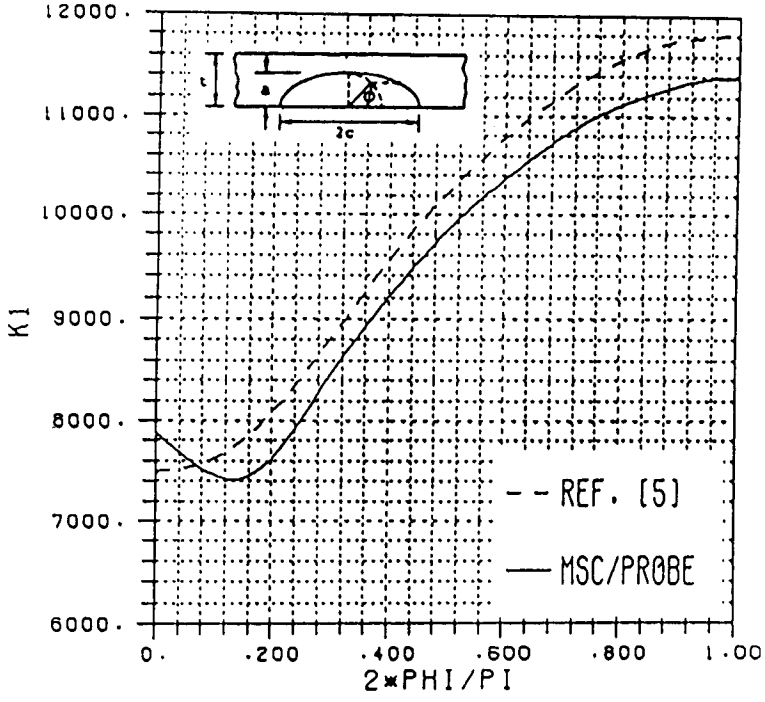

FIGURE 4.10: K_I RESULTS ALONG THE CRACK FRONT

5.0 SUMMARY AND CONCLUSIONS

This paper has discussed the application of the Finite Element Method to fracture mechanics computations. Particular emphasis was placed on proper evaluation of the quality of the numerical solution. The p-version finite element program, MSC/PROBE, which has extensive quality control features, was used for this purpose.

Several examples were provided to demonstrate the use of **MSC/PROBE** for fracture mechanics computations. The examples included a cracked panel with tension and shear loading, an axisymmetric solid rod with an imbedded penny shaped crack loaded in tension, and a solid plate with a semi-elliptical surface crack loaded in shear and tension. The quality control procedures were outlined for each example, and the fracture mechanics results were provided.

The p-version of the finite element method, as implemented in **MSC/PROBE**, has been demostrated to be particularly well suited for fracture mechanics computations. The automatic fracture mechanics extraction methods used in the planar and axisymmetric modules are extremely efficient and accurate. The quality control features that are provided, namely the global error in the energy norm, the elemental equilibrium, the inter-element stress continuity, and the convergence of the data of interest, all combine to provide the most powerful solution verification that can be found in finite elements today.

6.0 REFERENCES

[1] Szabó, B. and Babuška, I., "Computation of the Amplitude of Stress Singular Terms for Cracks and Reentrant Corners.", ASTM STP 969, pp. 101-124, 1988

[2] Parks, D., "A Stiffness Derivative Finite Element Technique for Determination of Crack Tip Stress Intensity Factors.", Int. J. of Fracture, Vol. 10. No. 4, (1974)

[3] Tada, H., Paris, P., Irwin, G., "The Stress Analysis of Cracks Handbook", Missouri: Paris Productions Inc., 1985.

[4] Paris, P., Sih, G., "Stress Analysis of Cracks", American Society for Testing and Materials, Special Technical Publication 381, 1970.

[5] Raju, I. S., Newman, J. C. Jr., "Stress Intensity Factors for a Wide Range of Semi-Elliptical Surface Cracks in Finite Thickness Plates.", Engineering Fracture Mechanics, Vol. II, pp. 817-829, 1979.

[6] Tan, P. W., Raju, I. S., Shivakumar, K. N., Newman, J. C. Jr., "A Re-evaluation of Finite Element Models and Stress-Intensity Factors for Surface Cracks Emanating from Stress Concentrations.",NASA Technical Memorandum 101527, 1988.